Green synthesis of zero-valent iron nanoparticles and loading effect on activated carbon for furfural adsorption

Yousef Rashtbari[1,2], Farooq Sher[3,*], Shirin Afshin[1], Asghar Hamzezadeh Bahrami[1], Shahin Ahmadi[4], Ofaira Azhar[5,6], Ayoob Rastegar[7], Soumya Ghosh[8], Yousef Poureshgh[1]

[1]*Department of Environmental Health Engineering, School of Health, Ardabil University of Medical Sciences, Ardabil 56189-85991, Iran*

[2]*Students Research Committee, Faculty of Health, Ardabil University of Medical Sciences, Ardabil 56189-85991, Iran*

[3]*Department of Engineering, School of Science and Technology, Nottingham Trent University, Nottingham NG11 8NS, United Kingdom*

[4]*Department of Environmental Health, Zabol University of Medical Sciences, Zabol 9861615881, Iran*

[5]*Department of Chemical Engineering, School of Chemical and Materials Engineering, National University of Sciences and Technology, Islamabad 44000, Pakistan*

[6]*International Society of Engineering Science and Technology, United Kingdom*

[7]*Department of Environmental Health, Sabzevar University of Medical Sciences, Faculty of Health, Sabzevar 319, Iran*

[8]*Department of Genetics, Faculty of Natural and Agricultural Sciences, University of the Free State, Bloemfontein 9300, South Africa*

***Corresponding author:**

Dr. F. Sher
Assistant Professor
Department of Engineering, School of Science and Technology
Nottingham Trent University
Nottingham
NG11 8NS
UK
E-mail address: Farooq.Sher@ntu.ac.uk
Tel.: +44 (0) 115 84 86679

Abstract

The adsorption techniques are extensively used in dyes, metronidazole, aniline, wastewater treatment methods to remove certain pollutants. Furfural is organic in nature, considered a pollutant having a toxic effect on humans and their environment and especially aquatic species. Due to distinct characteristics of the adsorption technique, this technique can be utilized to adsorb furfural efficiently. As an environmentally friendly technique, the pomegranate peel was used to synthesized activated carbon and nanostructure of zerovalent iron impregnated on the synthesized activated carbon. The physicochemical and crystallinity characterization was done using Fourier transmission infrared spectroscopy (FTIR), X-ray diffraction (XRD), Brunauer–Emmett–Teller (BET), and Field emission scanning electron microscopy (FESEM). The nanoparticles are porous in structure having 821.74 m^2/g specified surface area. The maximum amount of the adsorbent pores in the range of 3.08 nm shows the microporous structure and enhancement in adsorption capacity. The effects of increment in concentration of adsorbent, pH, reaction contact time and adsorbent dose, isothermal and kinetic behaviour were investigated. At the UV wavelength of 227 nm furfural adsorption was detected. The separation of the furfural from the aqueous solution was calculated at the 1 h reaction time at the composite dosage of 4 g/L, 250 mg/L adsorbent concentration and pH kept at 7. The 81.87% is the maximum removal attained by the nanocomposite in comparison to the activated carbon is 62.06%. Furfural adsorption was also analyzed by using the equations of isothermal and kinetics models. The adsorption process analysis depends on the Freundlich isotherm and Intra-particle diffusion than the other models. The maximum adsorbent of the composite was determined by the Langmuir model which is 222.22 mg/g. The furfural removal enhances as the adsorbent dose enhances. The developed zerovalent

iron nanoparticles incorporated on activated carbon (AC/nZVI) from pomegranate peel extract are feasible as an efficient and inexpensive adsorbent to eliminate furfural from a liquid solution.

Keywords: Pollutants; Pomegranate extract; Zero valent iron nanoparticles (nZVI); Wastewater treatment; Furfural removal; Activated carbon; Green Synthesis and Low-cost adsorbents

1 Introduction

The water sources are polluted by the presence of toxic materials, and substances. Complex chemical compounds of various industries such as petrochemicals, oil refineries, process units, and chemical production are the main contaminants and these industries have always been considered as a major source of environmental pollutants, especially for soil and water resources (Chen, Liang et al. 2019). Arsenic, hexavalent chromium (VI), lead and mercury are complex heavy metals among the wide range of elements and should be removed from the wastewater. 2-Furaldehyde (Furfural; $C_5H_4O_2$) is used on a large scale in oil refineries, petrochemical industries, paper, and cardboard and is present in their wastewater of about 100-1200 mg/L limited (Zhang, Jiang et al. 2021). Furfural is the family of the aldehydes and furans, in which furan bond with hydrogen at 2-substituted positions. Furfural is a bi-furfural liquid and oil that has an almond odour, rapidly turns to yellow furfural upon contact with air and water-soluble (Tarazanov, Grigoreva et al. 2020).

Human exposure can occur through inhalation, swallowing, skin or eye contact, or absorption through the skin. Furfural (concentrations of 1.9-14 ppm) has caused headaches, redness of the eyes, and tearing in some workers exposed to it. Exposure to higher concentrations causes pulmonary edema in lungs (JAFARIAN, MALMASI et al. 2011). Several methods such as catalytic and photocatalytic methods, extraction from nano filtration solvents, cyclic biological

reactor (CBR), biological degradation methods, and adsorption process. have been studied for furfural removal (Mao, Zhang et al. 2012). Studies have shown that furfural biodegradation includes both aerobic and anaerobic approaches, which are expensive (Sun, Liao et al. 2020). Furthermore, biodegradation of furfural removal is practically impossible due to the influence of various parameters and toxicity of furfural at high concentrations (Zhang, Zhu et al. 2011). As well as difficulties in degradability and toxicity in the petrochemical industry waste compounds decrease biodegradability which caused severe pollution in environment.

Nanotechnology in adsorption has become promising for the separation of furfural. Several kinds of adsorbents such as nanoparticles, magnetic adsorbents, cheap adsorbents, bio-adsorbents, and carbon nanotubes have been fabricated and tested for furfural elimination (Alaei Shahmirzadi, Hosseini et al. 2018). Nanotechnology is the study of materials that are <100 nm in size, and their physical, chemical and biological properties are fundamentally different from their origin. Polyol method, micro emulsions, thermal decomposition, electrochemical synthesis, sonochemical reduction and gamma radiation and many other are the proposed methods for the synthesis of nanoparticles (Ganguly, Das et al. 2017). Many of these methods are not efficient enough due to particle size, shape, and stabilization (Crucho and Barros 2017). To restraint the growth, shape of nanoparticles and keep them away from accumulating an efficient stabilizing agent and chemical reducing agents such as sodium borohydride and polyvinylpyrrolidone is used (Fazlzadeh, Khosravi et al. 2017).

However, there is considerable interest in the biogenesis of metal nanoparticles using plant and microbial extracts. Plant extract synthesis or the green synthesis of nanoparticles have been

prioritized because of the stability, low cost, energy efficient and non-toxic environment imparted by the nanoparticles (Gottimukkala, Harika et al. 2017). During the green synthesis, a redox reaction occurs in the saline solutions in which the plant extracts (reducing agents) transfer electrons to metal ions, and eventually, metal nanoparticles are produced. In this method, no pressure, energy, high temperature, and toxic chemicals are involved. Therefore, pose lower risks to humans and ecosystems and are cost-effective (Fazlzadeh, Khosravi et al. 2017). Today, zero-valent iron nanoparticles (nZVI) produced by natural materials (plant extracts) such as grape residue, grapefruit, eucalyptus leaves, and black tea extract have been used to synthesize (Ramezani, Kazemi et al. 2013).

To enhance the stability of nano molecules on supporting materials such as gold, oxides, titanium, polymers, fibres, metals and activated carbon acceleration of the removal of the nanomaterials from aqueous media is required. Among the above, the utilization of passive carbon has driven economic benefits and ecological considerations (Ghaedi, Ghayedi et al. 2013). Activated carbon (AC) synthesized by plant biomass has high active sites, cheap, renewability, favourable surface area, properties of surface chemistry, porous, and therefore has involved enormous consideration. However, commercial AC has been proved expensive. Therefore, there is an essence for economically affordable materials that could be an alternative for the commercially available AC. Algae, Fungi, coconut shell, corn, and lignin are the natural materials provide AC in extensive amount.

There are limited studies that have reported on the performance of AC prepared from pomegranate peel and the stabilization effect of nanoparticles on AC for furfural removal. Depending on the

above-mentioned information, this research investigates the synthesis of AC and nZVI nanoparticles through pomegranate peel. The nZVI nanoparticles are impregnated on the AC support. The key purpose of this research is to measure the furfural removal through nZVI nanoparticles. A systematic characterization was done by the Fourier transmission infrared spectroscopy (FTIR), X-ray diffraction (XRD), Brunauer–Emmett–Teller (BET), and Field emission scanning electron microscopy (FESEM). Nanocomposite added on the AC enhances the porosity and the activation sites to absorb the furfural pollutant. However, evaluation of the adsorbent dose and efficiency for the removal of furfural in synthetic aqueous solutions under the influence of several parameters such as reaction contact time, pH, dosage of adsorbent and initial concentration are analyzed. The experimental and adsorption results were also analyzed by isothermal and kinetic studies.

2 Materials and methods

2.1 Material

The furfural (MW; 96.08 g/mol), H_2SO_4 (purity; 97%), $FeCl_2$ (purity; 99.95%), and NaOH (purity; 50%) were procured from Merck, Germany. H_2SO_4 and NaOH were according to the pH of the furfural solution. In all the experimentations the distilled water was utilized twice obtained from Merck, Germany.

2.2 Preparation of the active carbon

In this study, pomegranate peel was used to prepare activated carbon (AC). In the first stage, the pomegranate skin was sliced into 0.5 cm pieces and impregnated with phosphoric acid. The impregnated skins were transferred to the reactor and placed at 800 °C for 2 h. The carbon was rinsed after the removal from the reactor and placed at 110 °C for 2 h in an oven to dry. Ultimately,

AC is separated by a sieve with a US mesh size between 20-30 and ready for use (Fazlzadeh, Khosravi et al. 2017).

2.3 Green synthesis of nZVI

Pomegranate peel extract was prepared by boiling for 60 min. $FeCl_2$ solution is added to 250 cc of distilled water with specified normality in the pomegranate peel extract. A vacuum pump is used to filter the nanoparticles from the obtained extract. The appearance of a darker colour shows the formation of zero-capacity iron particles. The nanoparticles were then settled in the oven at 70 °C for 24 h to dry (Leili, Fazlzadeh et al. 2018).

2.4 Loading nZVI on AC

The composite was synthesized by adding nZVI nanoparticles 0.05 g in 200 cc of distilled water and was stirred for 10 min to attain a homogenous solution. Following this, AC 5 g was added to the rest of the solution at 250 rpm for 2 h. The composite was placed in the oven for 10 h at 95°C temperature (Saleh 2018).

2.5 Characterization

Brunauer–Emmett–Teller (BET) was used to observe the surface area, pore volume and diameter of the AC and zero-valent iron nanoparticles (nZVI)by nitrogen gas adsorption analysis(Wu, Yang et al. 2013). The characterization of the adsorbent was performed by field emission scanning electron microscopy (FESEM) at the same magnification (Mortazavian, An et al. 2018). To discover the functional groups on the nanocomposite surface, Fourier transmission infrared spectroscopy (FTIR) analysis from 500-4000 cm^{-1} range was carried out by Perkin Elmer Spectrum. X-ray diffraction (XRD) of the composite was determined by Philips PNA-analytical diffractometer at an angle in the range of 2θ=10-80. The residual furfural concentration was measured by DR5000HACH spectrophotometer at 277 nm (Kakavandi, Kalantary et al. 2014).

2.6 Batch furfural adsorption studies

In the present study, 0.1 M H_2SO_4 and NaOH were used to align the pH. The furfural homogenous dilute solution was prepared. The adsorption study was performed with a pH change from (3 to 11) amount of adsorbent (0.5 to 6 g/L), furfural concentration (100 to 350 mg/L) and contact time (5 to 120 min) (Doddapaneni, Jain et al. 2018). The removal efficiency and the amount of furfural adsorption in the unit mass adsorbent after the process of adsorption were calculated using Eq. (1) and (2) respectively (Akram, Xu et al. 2021).

$$R\ (\%) = \frac{(C_0 - C_f)}{C_0} \times 100 \quad (1)$$

$$q_{e=} \frac{(C_{0-} C_e)V}{M} \quad (2)$$

where and the initial furfural concentration (C_0) and equilibrium liquid phase concentration (C_e) of furfural in mg/L, C_f is the final furfural concentration, The mass of AC/nZVI (g) and volume (V) of the solution (L).

2.7 Evaluation of zero charge point (pHpzc)

0.1 M NaCl about 50 mL of solution was poured into 150 mL Erlenmeyer flakes with the adjustment of pH with H_2SO_4 and NaOH in the range of 2-12. 0.04 g of nanocomposite was added to the NaCl solutions and kept on stirring for 48 h. The pH was analysed and the curve final pH (pH_f) versus initial pH (pH_i) was plotted. The curve shows the point that intersects the bisector was identified as the pH_{pzc} nanocomposite (Rafiaee, Samani et al. 2020).

3 Results and discussion

3.1 Adsorption and morphological analysis of composites

The FTIR analysis from 500-4000 cm^{-1} of AC and AC/nZVI composites are shown in Fig. 1(a). The adsorption bands at 900-1300 cm^{-1} belong to functional groups consisting of phosphorus,

192 which are the activation of phosphoric acid (H_3PO_4) used in the synthesis process (Ghaedi,
193 Ghayedi et al. 2013). The wavelengths that appeared between 400-1800 cm^{-1} are Fe-O bonds
194 vibrations. The presence of nZVI can be verified from the presence of an absorption band at 506
195 cm^{-1} (Bhatia, Datta et al. 2018). The 3000-2800 cm^{-1} band in the AC/nZVI composite is correlated
196 to C-H alkanes band (Seliem, Mobarak et al. 2020). The O-H vibration is in the band 1342 cm^{-1}
197 due to the presence of the H_2O molecule is observed for AC and AC/nZVI (Aksu Demirezen,
198 Yıldız et al. 2019). Also, the peaks observed in bands 2925 cm^{-1} and 2850 cm^{-1} indicated the
199 involvement of C-H group from pomegranate skin extract for the formation of particles (Leili,
200 Fazlzadeh et al. 2018). Absorption peaks appear at the absorption wavelengths in 1030, 1456,
201 1634, 2932 and 3426 cm^{-1} corresponding to the functional groups of polyphenol compounds.
202
203 Therefore, it can be claimed that reducing the metal ion and converting it to nanoparticles and
204 stabilizing nanoparticle polyphenols play a double purpose (Sun, Cai et al. 2014). Some peaks
205 disappeared after nZVI coverage in AC and decreased irregularity in the AC/nZVI spectrum.
206 Overall, nZVI coverage on AC has been successful. The XRD measurements were done to analyze
207 the crystalline or amorphous structure of the synthesized AC and AC/nZVI nanocomposites. Fig.
208 1(b) displays the XRD patterns of AC and AC/nZVI some prominent peaks indicate that the
209 adsorbent owns a crystalline structure that improves the process of adsorption. The XRD
210 diffraction peaks in both patterns, the broad peaks at 2Θ values below 22° correspond to the
211 presence of AC (Nasrullah, Saad et al. 2019). However, the high-intensity diffraction peaks at 2Θ
212 values above 25° indicate the clear presence of nZVI. The low-intensity peaks at 2Θ value of 34°,
213 48°, 56°, and 72° indicate the presence of nZVI which is also determined by FTIR and slightly

oxidized with AC (Fazlzadeh, Rahmani et al. 2017). Through this result, it was revealed that the AC/nZVI are perfectly index crystalline in nature.

SEM analysis was done to determine the morphology of both AC and nZVI. Fig. 2. shows the results of the morphology of the adsorbent surface. Fig. 2(a), shows that pomegranate extract has been successful to synthesize AC and the surface of AC has a favourable porosity. These cavities provide a good opportunity for nZVI nanoparticles to be trapped inside (Akram, Xu et al. 2020). In Fig. 2(b) and c nZVI nanostructures could be seen as small white particles on the AC support. The nanoparticles have different shapes, non-uniform, and void space. These nanoparticles are dispersed and evenly distributed on the AC which significantly increases the absorption rate of the nanocomposites. nZVI nanoparticles stability on AC partially blocks surface porosity, probably because zero-capacity iron nanoparticles cannot enter the internal cavities of AC tissue and therefore remain on the outer surface (Abu-Dalo, Jaradat et al. 2019). The FESEM of the fixed nanoparticles indicates that the porosity composite has a suitable specific surface area and the zero-capacity iron nanoparticles are well stabilized on the AC (Sravani, Raghavendra et al. 2020).

BET analysis was performed to examine the pore volume and surface area by assessing the volume of nitrogen gas (N_2) absorbed and desorbed by the material surface at a constant temperature of liquid nitrogen (77 K) (Esmaeili Bidhendi, Poursorkh et al. 2020). This analysis was performed by BET device Quanta Chrome Instruments, CHEMBET 3000 was used for analysis. Fig. 3 displays the BET analysis of AC/nZVI nanocomposite. It can be seen through the surface analysis graph that adsorbed volume of AC/nZVI is more than AC which reveals that nanocomposites have more adsorption capacity than AC. Table 1, shows that the nanocomposite AC/nZVI porosity is more

than AC. The specific surface area of AC and nanocomposite is calculated as 731.12 and 821.74 m^2/g, respectively. The maximum number of adsorbent pores was in the range of 3.08 nm, which indicates the microscopic structure .This result explains that by adding nZVI to the AC, the surface-modified and the adsorbent surface area increased that ultimately effects the absorption rate (Mohseni, Khalilzadeh et al. 2020).

3.2 Effect of pH on adsorption capacity

pH is the most important parameter in the adsorption process. Fig. 4 displays the results of the pH influence and concentration furfural. Fig. 4(a) shows the relation of the initial pH with the final pH. Initial pH shows a constant increase in adsorption rate upon an increment of the as compared to the pH_f. Further elaboration of the pH is done with the help of Fig. 4(b). In Fig. 4(b) data shows that increasing the pH from 2 to 12, the adsorption of furfural on nanocomposites AC/nZVI surface has also increased. With the reaction time of 1 h at a concentration of 250 mg/L the maximum removal was attained at pH 3,5,7,9, and 11. It was observed that the efficiency of removal under neutral pH parameters is slightly more than the alkaline and acidic conditions. pH at 7 was selected as the optimum pH. The AC-nZVI at $pH < pH_{pzc}$, had a positive charge and in $pH > pH_{pzc}$, it had a negative charge. As a result, in solutions with a $pH < 6.76$, the nanocomposite had a positive charge at its surface, while the furfural dye molecules were negatively charged. The decline in pH is due to the increase of H^+ ions in the solution. Furthermore, the formation of electrostatic attraction between the H^+ ion and the dye increases that ultimately increases the adsorption rate as well. If nanocomposite had a negative charge due to $pH > 6.76$, therefore, the anionic dye and the adsorbent repelled as reported earlier.

3.3 Effect of adsorbent dose

The adsorbent dose determines the adsorbent capacity for a given initial concentration of furfural. Fig. 5 shows the changes in the furfural adsorption process by the composite. It was discovered

that by increasing the adsorbent dose the furfural adsorption rate also increases. The furfural removal increased from 22.28 to 83.32% by an increment of the dosage from 0.5 to 6 g/L. It evaluated that removal percentage increase with adsorbent dose, but it could be 100% efficient. The q_{max} decreased with increasing dose therefore the q_{max} of furfural declined from 111.42 mg/g to 34.72 mg/g therefore, the optimum dose of 4 g/L was selected. With increasing the adsorbent dose, the increment in furfural efficiency is calculated, which changes faster in the 4 g/L adsorbent dose. After 4 g/L, the removal efficiency has been a slowdown and almost constant process. The increment in the adsorption rate is mainly based upon the surface sorption area and the interaction of the furfural with the nanocomposite. Increased furfural uptake occurs to increase the adsorbent dose due to the increment in positive sites, the increase in the adsorbent surface, and the presence of a strong driving force of the adsorbent to remove furfural (Fang and Yang 2021). Less active sites are present to adsorb the furfural molecules at low doses of adsorbent, which leads to a decrease in the efficiency of furfural removal (Shaban, Hassouna et al. 2017).

3.4 Effect of contact time

An influential factor in removal percentage is initial furfural concentration and reaction contact time with adsorbent. To determine the optimized contact time for solvent adsorption in the limit of 350-100 mg/L under pH kept at 7 and the amount of adsorbent 4 g/L, was evaluated at times from 0 to 120 min. The stirrer speed was kept at 250 rpm and the experimentation was performed at 25 °C temperature. The adsorbent removal was performed at high speed in 60 min and then increased with a gentle slope to 120 min and reached almost equilibrium. Therefore, the adsorbent optimal contact time was chosen to be 60 min to provide optimum time for furfural to be adsorbed on the surface. The rate of pollutant diffusion into the pores decreases, followed by the adsorption rate. Initially, the surfaces available to absorb the contaminant on the adsorbent are completely

free and as a result, the adsorbent is in contact with the contaminant with all surfaces and over time the available surfaces become less and thus the adsorption rate decreases (Fang and Yang 2021).

Fig. 6 shows furfural separation from aqueous solution by the initial concentration of the adsorbent. It was revealed that at the equilibrium time of 60 min the capacity of furfural removal was declined by increasing furfural concentration. As the furfural concentration increment from 100 to 250 mg/L, the furfural removal efficiency increased from 85.9 to 90.93%, respectively. By increasing the initial furfural concentration, the number of collisions increases with the nanoparticles which increase the rate of adsorption and render a high surface area for adsorption of furfural (Fazlzadeh, Rahmani et al. 2017). This may be owed to the several active sites on the adsorbent that becomes saturated at higher concentrations of furfural. In other words, at low concentrations, the availability of the active AC/nZVI sites to the furfural molecules is more than when high concentrations of furfural are involved (Adio, Omar et al. 2017).

3.5 Isothermal models

Isotherm plots for furfural adsorption are shown in Fig. 7 at pH 7, AC/nZVI dose of 4 g/L and 25 ± 2 ˚C. Table 2 displays the isotherm parameters at ideal conditions. Providing the R^2 values obtained for the tested isotherm models, the Langmuir and Freundlich calculations firmly related to the experimental result. Langmuir and Freundlich describe a method of chemical adsorption through their equations represented in Table 2. (Zhang, Yan et al. 2019). The Freundlich models are acceptable for furfural adsorption through AC/nZVI adsorbent. The q_{max} obtained from the Langmuir model for the nanocomposite 222.2 mg/g shows that adsorption increase as the dosage decreases. An adsorption intensity (n) of 1.74 within 1 to 10 ($1< n<10$) for furfural adsorption indicates a desirable adsorption process on AC/nZVI (Shu, Ji et al. 2020). Fig. 7 displays the R^2 values and parameters for Langmuir and Freundlich isotherm models are shown in Fig. 7

calculated by plotting 1/Ce versus 1/qe Fig. 7(a), and $\log_{Ce}$ versus $\log_{qe}$ Fig. 7(b), from slopes and intercepts. The isotherm graphs for adsorption of furfural by AC/nZVI nanoparticles at the appropriate pH 7, 4 g/L dosages, and temperature of 25 ± 2 ˚C as shown in Fig. 8. The straight line obtained for both the models represent the adsorption capacity and the adsorbed molecules have the same structure, and these models are efficient to remove the furfural(Danalıoğlu, Bayazit et al. 2017). The intensity and the adsorption capacity obtained from Freundlich is more than the Langmuir which make this model more efficient for the nanocomposite to remove furfural.

3.6 Kinetic studies

Kinetic experiments are conducted to track the mechanism that governs an adsorption process. To test the kinetic data by the pseudo-first-order, pseudo-second-order, and intraparticle diffusion models were used. The equations of linear kinetic models with kinetic parameter definition are given in Table 3. The kinetic studies are displayed in Fig. 9. Log (q_e–q_t) versus t estimated the Pseudo-first order from the intercepts and slopes of plots shown in Fig. 9(a), pseudo-second-order are estimated from slops and intercepts of plots between t/qt versus t from Fig. 9(b). The findings obtained on linear adsorption kinetics are summarized in Table 3. The kinetic parameters were derived from the kinetic models' plots at maximum pH 7 conditions and 4 g/L doses of AC/nZVI. The most suitable model was selected by the regression coefficients R^2. The regression coefficients (R^2) verified the correlation between the predicted kinetic model values and the experimentation results. With the help of the R^2 value, the pseudo-second-order kinetic model is estimated fit to characterize the kinetic experimentation with its values of R^2 closer to unity. This means that the adsorption of furfural to AC/nZVI is a chemical adsorption form (Fazlzadeh, Ansarizadeh et al. 2018).

3.7 Adsorbent recyclability

The adsorbent recovery process is considered to get their economic value and solve operational problems. AC/nZVI was recovered using 0.1 M NaOH solution. Fig. 10, shows the five recovery cycles, suggesting that the restored adsorbent already has a high potential to adsorb the furfural and can be used regularly. The furfural removal performance was 91%, which decreased to 81.74% after the first cycle. The NaOH and the furfural in the active AC/nZVI sites interact, and the furfural is isolated from the active sites. Therefore, nanocomposite has a high potential for wastewater treatment and in the pharmaceutical industry. It can be reused to maintain the furfural removal efficiency after five consecutive periods by recovering the adsorbent. It is also cost-effective and therefore very necessary for industrial applications to prevent secondary pollution in the treatment of wastewater (De Gisi, Lofrano et al. 2016).

3.8 Comparison of AC-nZVI nanocomposites

The performance of furfural removal obtained using AC-nZVI from its aqueous solution and the deposition of furfural in the presence of AC/nZVI in Fig. 11 using AC as an adsorbent under the same condition can be compared with other adsorbents. Furfural adsorption of 81.87% and 62.06% were obtained using adsorption AC/nZVI and AC, respectively. Using AC/nZVI, furfural adsorption of 81.87% was attained within 60 min. The improvement in surface adsorption of the AC is due to the AC and nZVI interaction. Presently, from several methods, adsorption is considered an auspicious treatment to remove many defiant furfurals. Based on Table 4, furfural removal has been studied by many researchers in aqueous environments via several adsorbents such as torrefied biomass, MCM-48, and Organo bentonite. These adsorbents give the solvent removal up to 61% which is low than the results obtained by nZVI that is up to 81.87%. On the other end, the separation of the furfural desorption process is a favourable method. Moderate costs and nontoxicity are the benefits of the desorption method as compared to other methods. with

highly separation capacity, other benefits include its low costs and non-toxicity. in comparison to other adsorbents, it is a new composite that can be used for adsorption processes but still there is room for improvement to achieve better results.

4 Conclusion

The adsorption of furfural onto AC/nZVI nanoparticles was examined in this report. The findings of this analysis show that furfural can be extracted in a very short time by the process of adsorbing on AC/nZVI nanoparticles. The calculation of several operating conditions like pH (2-12), reaction contact time (5-120 min), dosage (0.5–6 g/L), temperature (298K), and concentration of furfural (100–350 mg/L) on AC and nanocomposite adsorbent were studied. Furthermore, as compared to the AC the removal efficiency by AC/nZVI is 81.46% which was observed at the best conditions such as furfural at maximum concentration 250 mg/L, pH of 7, and AC/nZVI with 4 g/L dosage and 1 h reaction contact time. Results revealed that the process of furfural adsorption on AC/nZVI is dependent on the Freundlich adsorption isotherm models. Monolayer maximum 222.22 mg/g is the adsorption capacity of AC/nZVI determined by the isotherm Freundlich model. With the estimated values of the regression coefficients (R^2) the adsorption kinetic data was fitted best into the pseudo-second-order model. AC/nZVI with a very high capability is nevertheless convenient economically to remove various contaminants from water. It could be concluded that the synthesized AC/nZVI could be utilized as an operational adsorbent for furfural ions separation from liquid solutions. In future, the nanoparticles can be incorporated into the adsorptive membranes and nZVI can be modified for the removal of heavy metals with furfural from wastewater.

Acknowledgements

This research received funding from Project no. IR.ARUMS.REC.1398.018 (Ardabil University of Medical Sciences). The authors are grateful for the financial supports the Engineering and Physical Sciences Research Council (EPSRC) UK. The authors sincerely appreciate the monetary and instrumental supports from Ardabil University of Medical Sciences.

References

Abu-Dalo, M., A. Jaradat, B. A. Albiss and N. A. F. Al-Rawashdeh (2019). "Green synthesis of TiO2 NPs/pristine pomegranate peel extract nanocomposite and its antimicrobial activity for water disinfection." Journal of Environmental Chemical Engineering **7**(5): 103370.

Adio, S. O., M. H. Omar, M. Asif and T. A. Saleh (2017). "Arsenic and selenium removal from water using biosynthesized nanoscale zero-valent iron: a factorial design analysis." Process Safety and Environmental Protection **107**: 518-527.

Akram, M., X. Xu, B. Gao, S. Wang, R. Khan, Q. Yue, P. Duan, H. Dan and J. Pan (2021). "Highly efficient removal of phosphate from aqueous media by pomegranate peel co-doping with ferric chloride and lanthanum hydroxide nanoparticles." Journal of Cleaner Production **292**: 125311.

Akram, M., X. Xu, B. Gao, Q. Yue, S. Yanan, R. Khan and M. A. Inam (2020). "Adsorptive removal of phosphate by the bimetallic hydroxide nanocomposites embedded in pomegranate peel." Journal of Environmental Sciences **91**: 189-198.

Aksu Demirezen, D., Y. Ş. Yıldız, Ş. Yılmaz and D. Demirezen Yılmaz (2019). "Green synthesis and characterization of iron oxide nanoparticles using Ficus carica (common fig) dried fruit extract." Journal of Bioscience and Bioengineering **127**(2): 241-245.

Alaei Shahmirzadi, M. A., S. S. Hosseini, J. Luo and I. Ortiz (2018). "Significance, evolution and recent advances in adsorption technology, materials and processes for desalination, water softening and salt removal." Journal of Environmental Management **215**: 324-344.

Bhatia, D., D. Datta, A. Joshi, S. Gupta and Y. Gote (2018). "Adsorption study for the separation of isonicotinic acid from aqueous solution using activated carbon/Fe3O4 composites." Journal of Chemical & Engineering Data **63**(2): 436-445.

Chen, Y., W. Liang, Y. Li, Y. Wu, Y. Chen, W. Xiao, L. Zhao, J. Zhang and H. Li (2019). "Modification, application and reaction mechanisms of nano-sized iron sulfide particles for pollutant removal from soil and water: A review." Chemical Engineering Journal **362**: 144-159.

Crucho, C. I. and M. T. Barros (2017). "Polymeric nanoparticles: A study on the preparation variables and characterization methods." Materials Science and Engineering: C **80**: 771-784.

Danalıoğlu, S. T., Ş. S. Bayazit, Ö. Kerkez Kuyumcu and M. A. Salam (2017). "Efficient removal of antibiotics by a novel magnetic adsorbent: Magnetic activated carbon/chitosan (MACC) nanocomposite." Journal of Molecular Liquids **240**: 589-596.

De Gisi, S., G. Lofrano, M. Grassi and M. Notarnicola (2016). "Characteristics and adsorption capacities of low-cost sorbents for wastewater treatment: a review." Sustainable Materials and Technologies **9**: 10-40.

Doddapaneni, T. R. K. C., R. Jain, R. Praveenkumar, J. Rintala, H. Romar and J. Konttinen (2018). "Adsorption of furfural from torrefaction condensate using torrefied biomass." Chemical Engineering Journal **334**: 558-568.

Esmaeili Bidhendi, M., Z. Poursorkh, H. Sereshti, H. Rashidi Nodeh, S. Rezania and M. Afzal Kamboh (2020). "Nano-Size Biomass Derived from Pomegranate Peel for Enhanced Removal of

Cefixime Antibiotic from Aqueous Media: Kinetic, Equilibrium and Thermodynamic Study." International Journal of Environmental Research and Public Health **17**(12): 4223.
Fang, K. and R.-d. Yang (2021). "Modified activated carbon by air oxidation as a potential adsorbent for furfural removal." Alexandria Engineering Journal **60**(2): 2325-2333.
Fazlzadeh, M., M. Ansarizadeh and M. Leili (2018). "Data of furfural adsorption on nano zero valent iron (NZVI) synthesized from Nettle extract." Data in brief **16**: 341-345.
Fazlzadeh, M., R. Khosravi and A. Zarei (2017). "Green synthesis of zinc oxide nanoparticles using Peganum harmala seed extract, and loaded on Peganum harmala seed powdered activated carbon as new adsorbent for removal of Cr(VI) from aqueous solution." Ecological Engineering **103**: 180-190.
Fazlzadeh, M., K. Rahmani, A. Zarei, H. Abdoallahzadeh, F. Nasiri and R. Khosravi (2017). "A novel green synthesis of zero valent iron nanoparticles (NZVI) using three plant extracts and their efficient application for removal of Cr (VI) from aqueous solutions." Advanced Powder Technology **28**(1): 122-130.
Fazlzadeh, M., K. Rahmani, A. Zarei, H. Abdoallahzadeh, F. Nasiri and R. Khosravi (2017). "A novel green synthesis of zero valent iron nanoparticles (NZVI) using three plant extracts and their efficient application for removal of Cr(VI) from aqueous solutions." Advanced Powder Technology **28**(1): 122-130.
Ganguly, S., P. Das, M. Bose, T. K. Das, S. Mondal, A. K. Das and N. C. Das (2017). "Sonochemical green reduction to prepare Ag nanoparticles decorated graphene sheets for catalytic performance and antibacterial application." Ultrasonics Sonochemistry **39**: 577-588.
Ghaedi, M., M. Ghayedi, S. N. Kokhdan, R. Sahraei and A. Daneshfar (2013). "Palladium, silver, and zinc oxide nanoparticles loaded on activated carbon as adsorbent for removal of bromophenol red from aqueous solution." Journal of Industrial and Engineering Chemistry **19**(4): 1209-1217.
Gottimukkala, K., R. Harika and D. Zamare (2017). "Green synthesis of iron nanoparticles using green tea leaves extract." J. Nanomed. Biother. Discov **7**: 151.
Hosseini, S., S. Amini, A. Khodabakhshi, E. Bagheripour and B. Van der Bruggen (2018). "Activated carbon nanoparticles entrapped mixed matrix polyethersulfone based nanofiltration membrane for sulfate and copper removal from water." Journal of the Taiwan Institute of Chemical Engineers **82**: 169-178.
JAFARIAN, M. E., S. MALMASI, S. M. MONAVARI and S. A. JOZI (2011). "Survey of the environmental impact of the petrochemical industry of Mahshahr economic special zone using the analytic hierarchy process method."
Kakavandi, B., R. R. Kalantary, M. Farzadkia, A. H. Mahvi, A. Esrafili, A. Azari, A. R. Yari and A. B. Javid (2014). "Enhanced chromium (VI) removal using activated carbon modified by zero valent iron and silver bimetallic nanoparticles." Journal of environmental health science and engineering **12**(1): 1-10.
Leili, M., M. Fazlzadeh and A. Bhatnagar (2018). "Green synthesis of nano-zero-valent iron from Nettle and Thyme leaf extracts and their application for the removal of cephalexin antibiotic from aqueous solutions." Environmental technology **39**(9): 1158-1172.

458 Mao, L., L. Zhang, N. Gao and A. Li (2012). "FeCl3 and acetic acid co-catalyzed hydrolysis of
459 corncob for improving furfural production and lignin removal from residue." Bioresource
460 technology **123**: 324-331.
461 Mebrek, O. R. and Z. Derriche (2010). "Removal of furfural from aqueous solutions by adsorption
462 using organobentonite: isotherm and kinetic studies." Adsorption Science & Technology **28**(6):
463 533-545.
464 Mohseni, M. S., M. A. Khalilzadeh, M. Mohseni, F. Z. Hargalani, M. I. Getso, V. Raissi and O.
465 Raiesi (2020). "Green synthesis of Ag nanoparticles from pomegranate seeds extract and synthesis
466 of Ag-Starch nanocomposite and characterization of mechanical properties of the films."
467 Biocatalysis and Agricultural Biotechnology **25**: 101569.
468 Mortazavian, S., H. An, D. Chun and J. Moon (2018). "Activated carbon impregnated by zero-
469 valent iron nanoparticles (AC/nZVI) optimized for simultaneous adsorption and reduction of
470 aqueous hexavalent chromium: Material characterizations and kinetic studies." Chemical
471 Engineering Journal **353**: 781-795.
472 Nasrullah, A., B. Saad, A. H. Bhat, A. S. Khan, M. Danish, M. H. Isa and A. Naeem (2019).
473 "Mangosteen peel waste as a sustainable precursor for high surface area mesoporous activated
474 carbon: Characterization and application for methylene blue removal." Journal of Cleaner
475 Production **211**: 1190-1200.
476 Rafiaee, S., M. R. Samani and D. Toghraie (2020). "Removal of hexavalent chromium from
477 aqueous media using pomegranate peels modified by polymeric coatings: Effects of various
478 composite synthesis parameters." Synthetic Metals **265**: 116416.
479 Ramezani, F., B. Kazemi and A. Jebali (2013). "Biosynthesis of silver nanoparticles by
480 Leishmania sp." New Cellular and Molecular Biotechnology Journal **3**(9): 107-111.
481 Saleh, T. A. (2018). "Simultaneous adsorptive desulfurization of diesel fuel over bimetallic
482 nanoparticles loaded on activated carbon." Journal of Cleaner Production **172**: 2123-2132.
483 Seliem, M. K., M. Mobarak, A. Selim, E. Mohamed, R. A. Halfaya, H. K. Gomaa, I. Anastopoulos,
484 D. A. Giannakoudakis, E. C. Lima and A. Bonilla-Petriciolet (2020). "A novel multifunctional
485 adsorbent of pomegranate peel extract and activated anthracite for Mn (VII) and Cr (VI) uptake
486 from solutions: Experiments and theoretical treatment." Journal of Molecular Liquids **311**:
487 113169.
488 Shaban, M., M. E. M. Hassouna, F. M. Nasief and M. R. AbuKhadra (2017). "Adsorption
489 properties of kaolinite-based nanocomposites for Fe and Mn pollutants from aqueous solutions
490 and raw ground water: kinetics and equilibrium studies." Environmental Science and Pollution
491 Research **24**(29): 22954-22966.
492 Shah, P. V. and S. J. Rajput (2017). "A comparative in vitro release study of raloxifene
493 encapsulated ordered MCM-41 and MCM-48 nanoparticles: A dissolution kinetics study in
494 simulated and biorelevant media." Journal of Drug Delivery Science and Technology **41**: 31-44.
495 Shu, Y., B. Ji, B. Cui, Y. Shi, J. Wang, M. Hu, S. Luo and D. Guo (2020). "Almond shell-derived,
496 biochar-supported, nano-zero-valent iron composite for aqueous hexavalent chromium removal:
497 performance and mechanisms." Nanomaterials **10**(2): 198.

Sravani, B., P. Raghavendra, Y. Chandrasekhar, Y. Veera Manohara Reddy, R. Sivasubramanian, K. Venkateswarlu, G. Madhavi and L. Subramanyam Sarma (2020). "Immobilization of platinum-cobalt and platinum-nickel bimetallic nanoparticles on pomegranate peel extract-treated reduced graphene oxide as electrocatalysts for oxygen reduction reaction." International Journal of Hydrogen Energy **45**(13): 7680-7690.

Sun, C., Q. Liao, A. Xia, Q. Fu, Y. Huang, X. Zhu, X. Zhu and Z. Wang (2020). "Degradation and transformation of furfural derivatives from hydrothermal pre-treated algae and lignocellulosic biomass during hydrogen fermentation." Renewable and Sustainable Energy Reviews **131**: 109983.

Sun, Q., X. Cai, J. Li, M. Zheng, Z. Chen and C. Yu (2014). "Colloids and surfaces a: physicochemical and engineering aspects green synthesis of silver nanoparticles using tea leaf extract and evaluation of their stability and antibacterial activity." Colloids Surf A Physicochem Eng Aspects **444**: 226-231.

Tarazanov, S., K. Grigoreva, A. Shipitcyna, O. Repina, M. Ershov, S. Kuznetsova and P. Nikulshin (2020). "Assessment of the chemical stability of furfural derivatives and the mixtures as fuel components." Fuel **271**: 117594.

Wu, X., Q. Yang, D. Xu, Y. Zhong, K. Luo, X. Li, H. Chen and G. Zeng (2013). "Simultaneous adsorption/reduction of bromate by nanoscale zerovalent iron supported on modified activated carbon." Industrial & Engineering Chemistry Research **52**(35): 12574-12581.

Zhang, H., M. Jiang, Y. Wu, L. Li, Z. Wang, R. Wang and G. Zhou (2021). "Development of completely furfural-based renewable polyesters with controllable properties." Green Chemistry **23**(6): 2437-2448.

Zhang, W., Y. Zhu, S. Niu and Y. Li (2011). "A study of furfural decarbonylation on K-doped Pd/Al2O3 catalysts." Journal of Molecular Catalysis A: Chemical **335**(1-2): 71-81.

Zhang, X., L. Yan, J. Liu, Z. Zhang and C. Tan (2019). "Removal of different kinds of heavy metals by novel PPG-nZVI beads and their application in simulated stormwater infiltration facility." Applied Sciences **9**(20): 4213.

List of Tables

Table 1. BET analysis of AC and AC/nZVI nanocomposites.

Material	S_{BET} (m^2/g)	S_{micro} (m^2/g)	S_{meso} (m^2/g)	V_{Total} (cm^3/g)	V_{micro} (cm^3/g)	V_{meso} (cm^3/g)	D_p (nm)
AC	731.12	524.13	213.26	0.55	0.23	0.31	3.01
AC/nZVI	821.74	591.29	234.52	0.63	0.26	0.36	3.09

Table 2. Equilibrium parameters isotherm models for furfural adsorption.

	Langmuir				**Freundlich**		
Equation	$\frac{C_e}{q_e} = \frac{C_e}{q_m} + \frac{1}{q_m K_L}$				$q_e = K_F C_e^{\frac{1}{n}}$		
	q_m(mg/g)	**K_L(L/mg)**	**R2**	**R_L**	**K_f [(mg/g) (mg/L)1/n]**	**n**	**R2**
Furfural	222.22	0.002	0.97	0.57	3.10	1.74	**0.9**9

Table 3. Kinetics parameters for pseudo-first-order and pseudo-second-order.

	Pseudo first order				**Pseudo second order**		
	$Log(q_e - q_t) = Log q_e - \frac{k_1 t}{2.303}$				$t/q_t = 1/k_{2p}q_e^2 + t/q_e$		
C_0 (mg/L)	**$q_{e,epx}$ (mg/g)**	**$q_{e1,cal}$ (mg/g)**	**k_1 (min^{-1})**	**R^2**	**$q_{e2,cal}$ (mg/g)**	**K_2 (mg/g.min)**	**R^2**
100	24.25	20.62	0.03	0.86	24.51	0.01	0.99
150	34.50	20.90	0.03	0.94	36.63	0.002	0.98
250	58.75	44.86	0.02	0.85	60.98	0.0009	0.95
350	69.54	52.47	0.01	0.75	70.92	0.0004	0.88

Table 4. Comparison of the present study adsorption of furfural onto various adsorbents with the literature.

Adsorbent material	Maximum removal (%)	Maximum q_{max} (mg/g)	Conditions	References
Activated Carbon	60	0.05	pH = 5.9 Adsorbent dosage = 10 g/L Initial concentration = 50mg/L Time = 60 min Temperature = 303 K	(Hosseini, Amini et al. 2018)
Torrefied Biomass	60	80	pH = 2 Adsorbent dosage = 250 g/L Initial concentration = 50 mg/L Time = 30 min	(Doddapaneni, Jain et al. 2018)
MCM-48	-	196.1	pH = 6 Adsorbent dosage = 0.1 g/L Initial concentration = 1000 mg/L Time = 1 h Temperature=298 K	(Shah and Rajput 2017)
AC/nZVI	81.3	222.22	pH = 7 Adsorbent dosage = 4 g/L Initial concentration = 250 mg/L Time = 60 min Temperature = 25 ± 2°C	This study
Organo bentonite	-	536.3	pH = 7 Adsorbent dose = 2 g/L Contact time = 6h Temperature = 30 ^{0}C Initial concentration = 100 mg/L	(Mebrek and Derriche 2010)

List of Figures

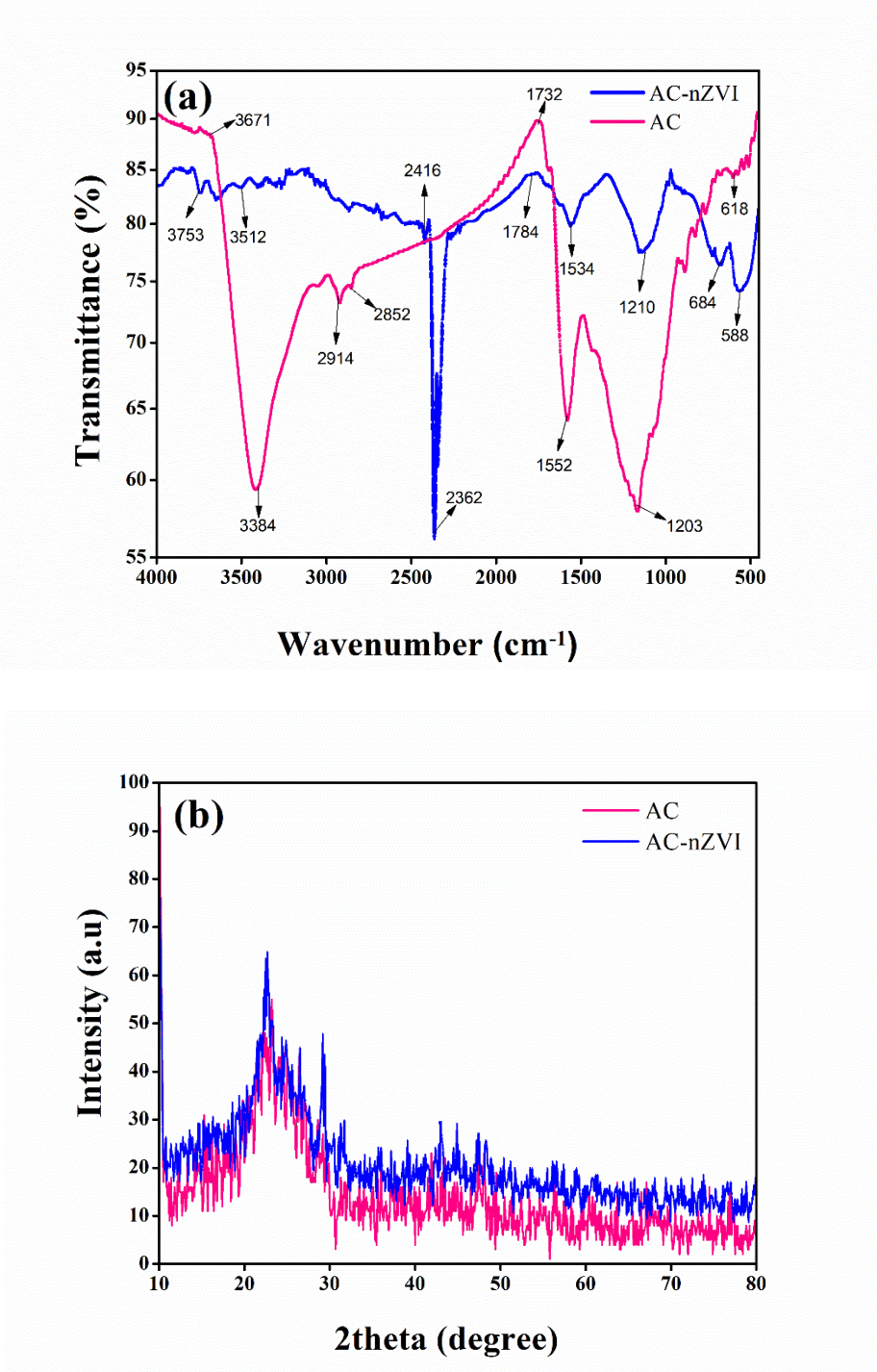

Fig. 1. Physicochemical analysis; (a) FTIR spectra of the AC and AC/nZVI nanoparticles; (b) XRD patterns of the AC and AC/nZVI nanocomposites.

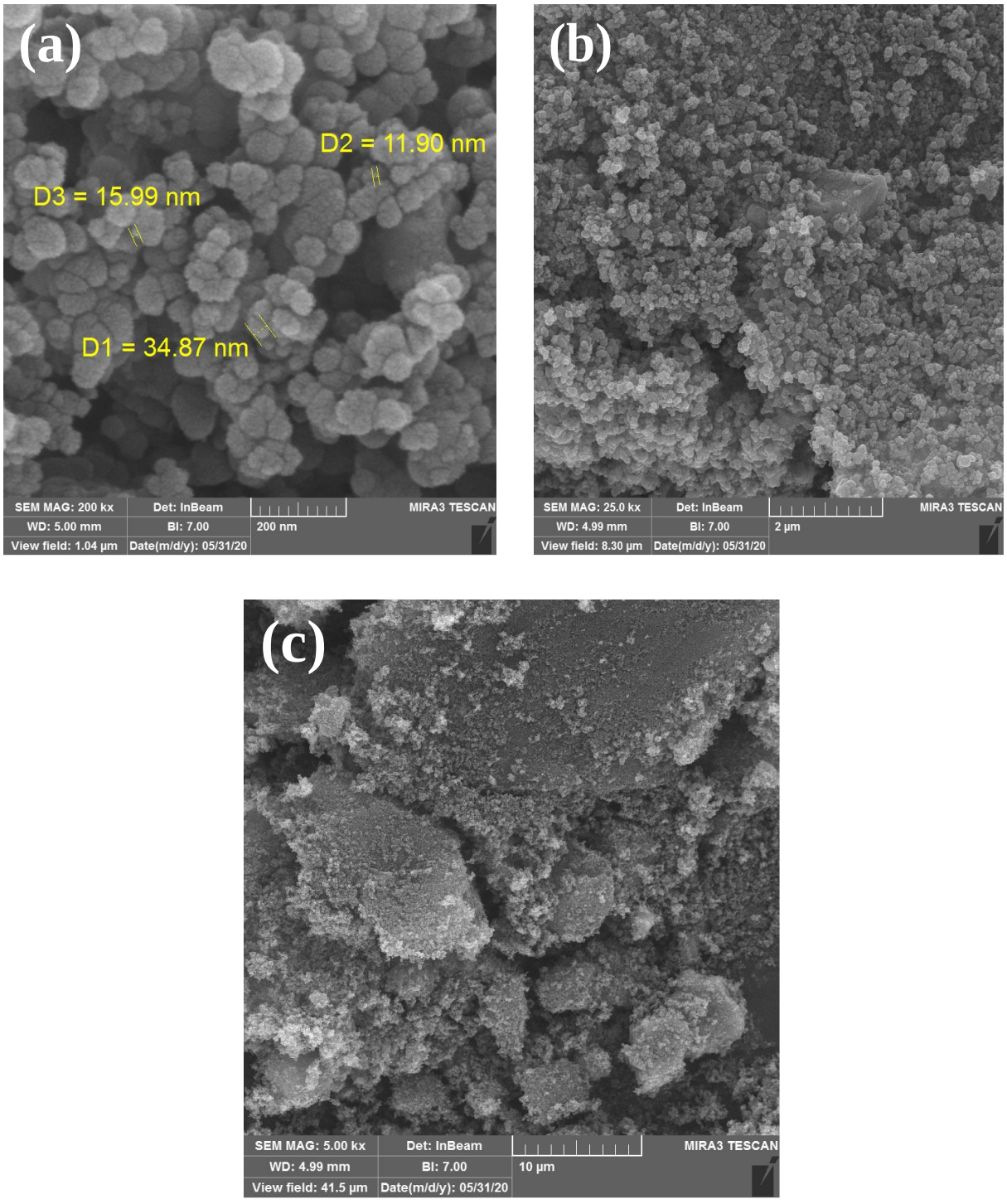

Fig.2. FE-SEM images; (a) Activated Carbon surface morphology; (b) and (c) Activated Carbon impregnated by nZVI nanoparticles.

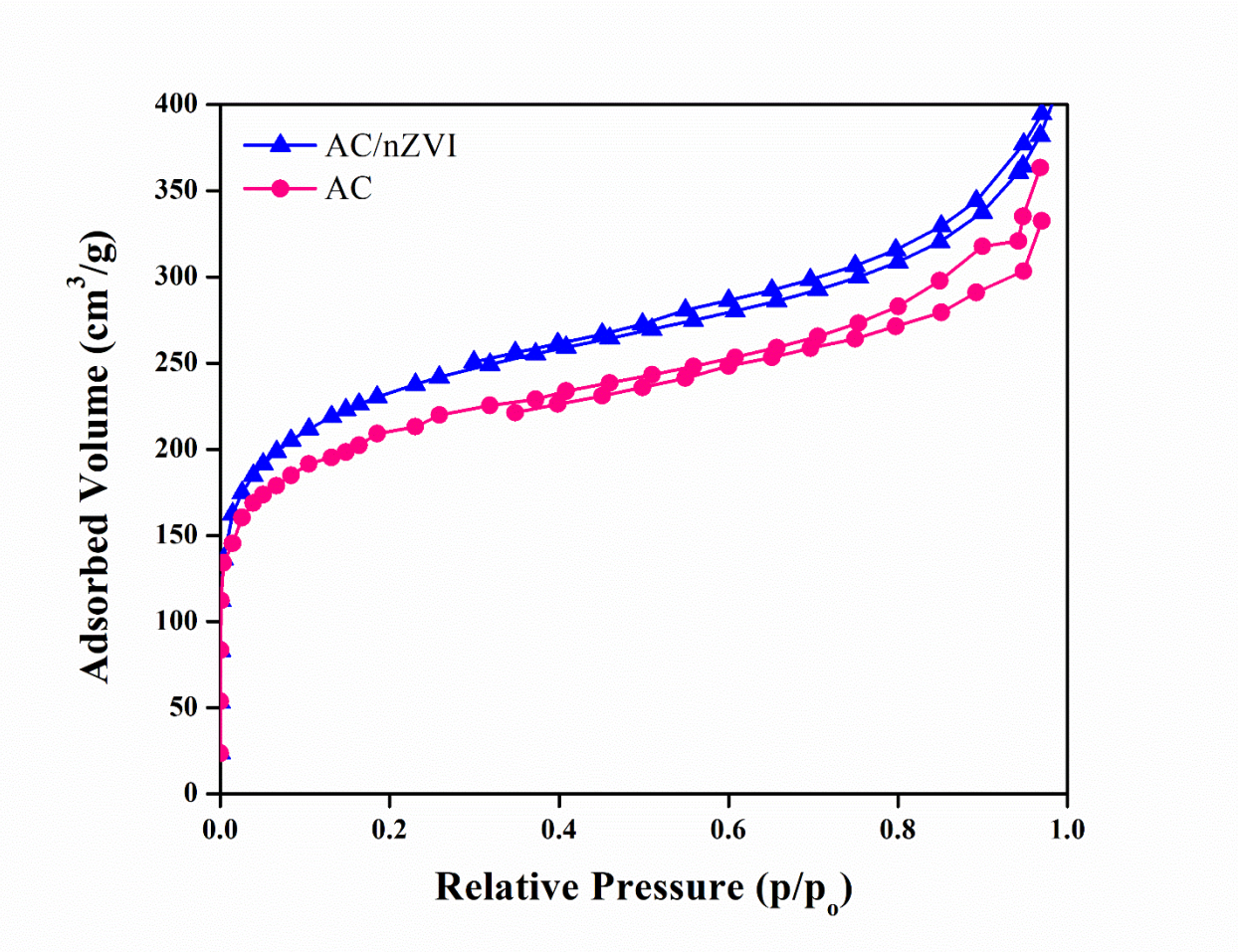

Fig. 3. Surface area analysis by BET characterization of AC and AC/nZVI nanocomposites.

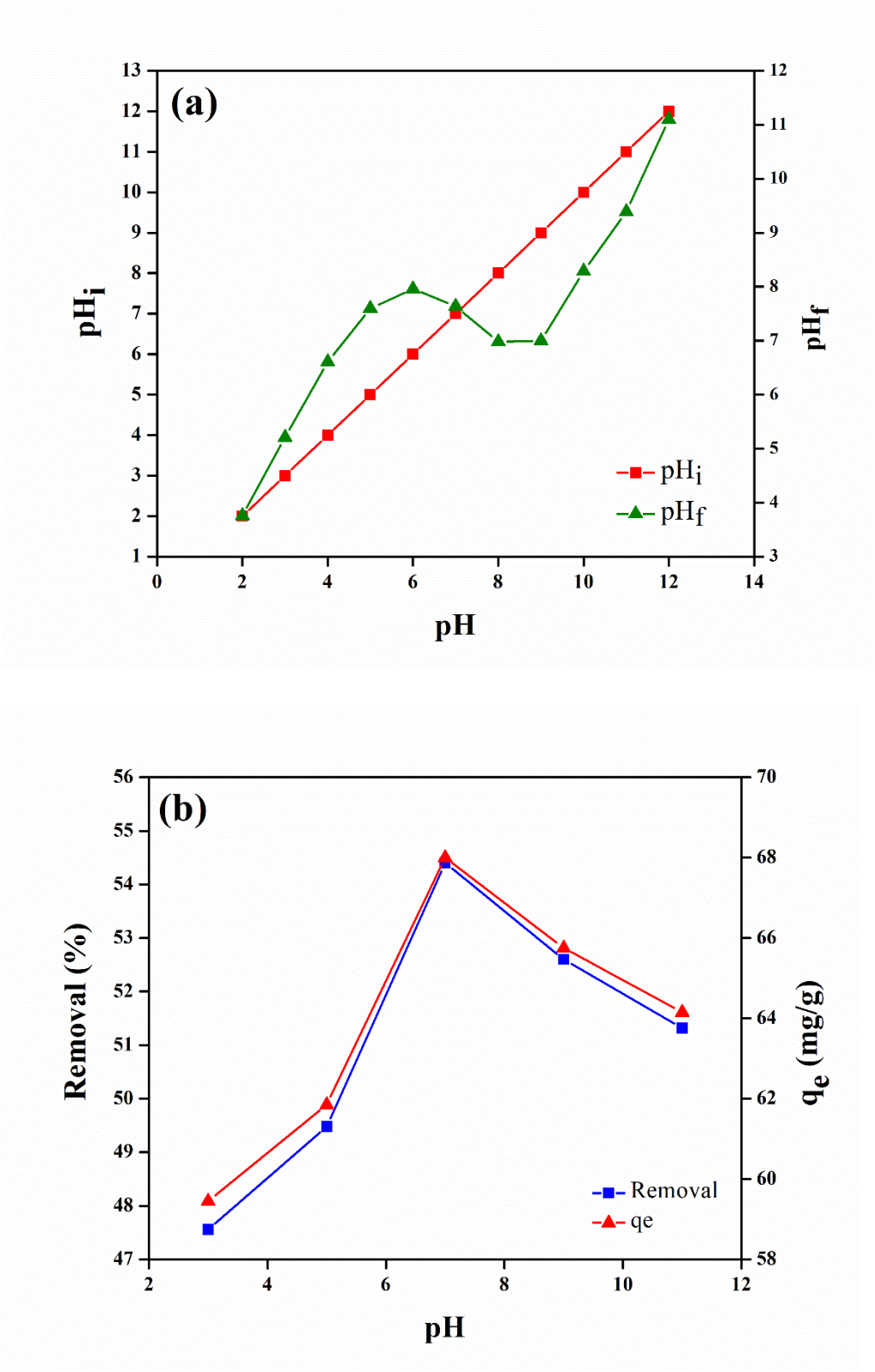

Fig. 4. pH improvement by the concentration removal of furfural; (a) pHpzc; (b) pH (C_0= 200 mg/L, Time=60 min, stirring speed = 250 rpm, Temp = 25 ± 2˚C).

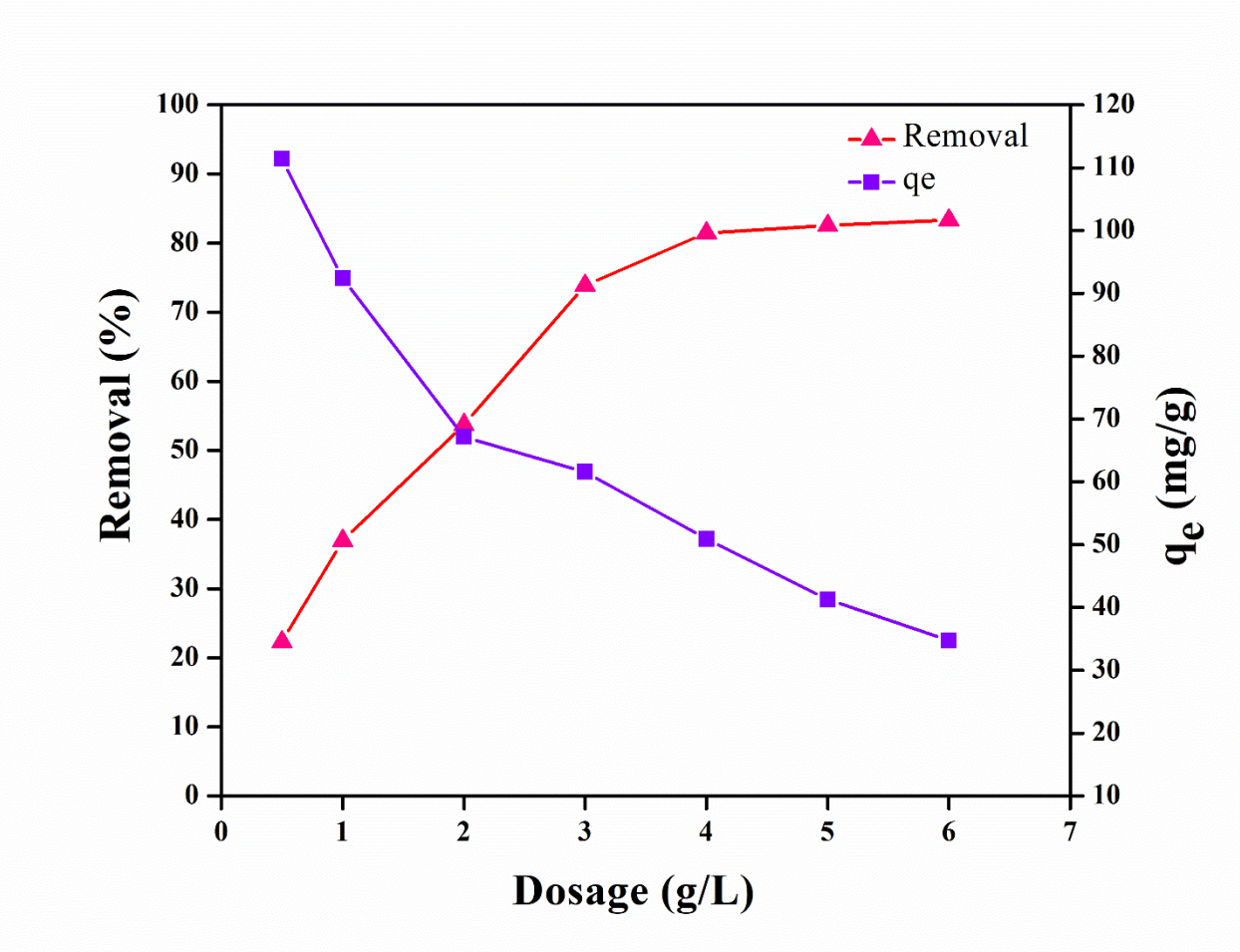

Fig. 5. The effect of the AC/nZVI dosage varies on the removal efficiency of furfural (C_0= 200 mg/L, Time=60 min, stirring speed = 250 rpm, Temp = 25 ± 2°C and pH = 7).

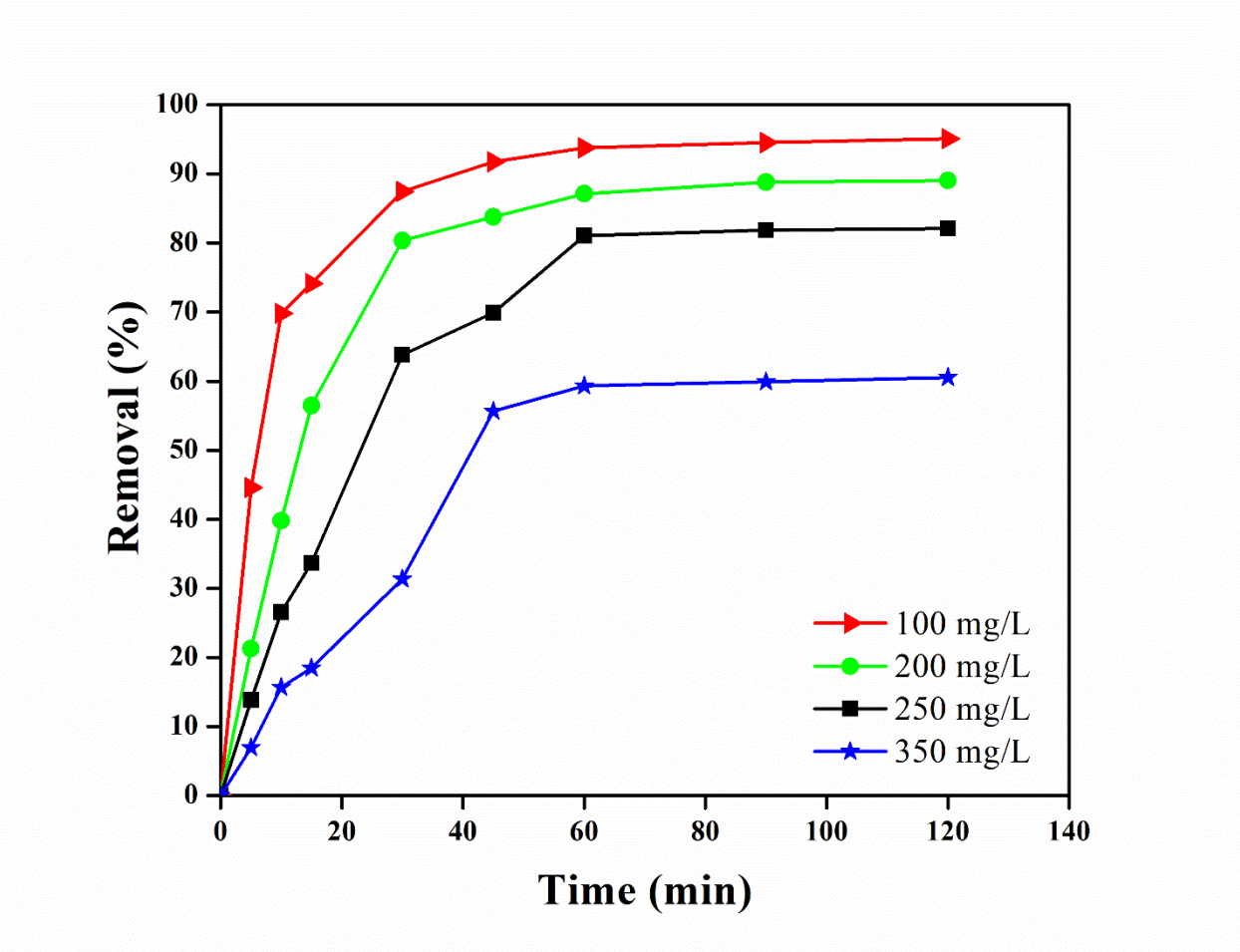

Fig. 6. Effect of contact time and the adsorption of furfural onto AC/nZVI nanoparticles (dose = 4 g/L, stirring speed = 250 rpm, Temp = 25 ± 2 ˚C, and pH =7).

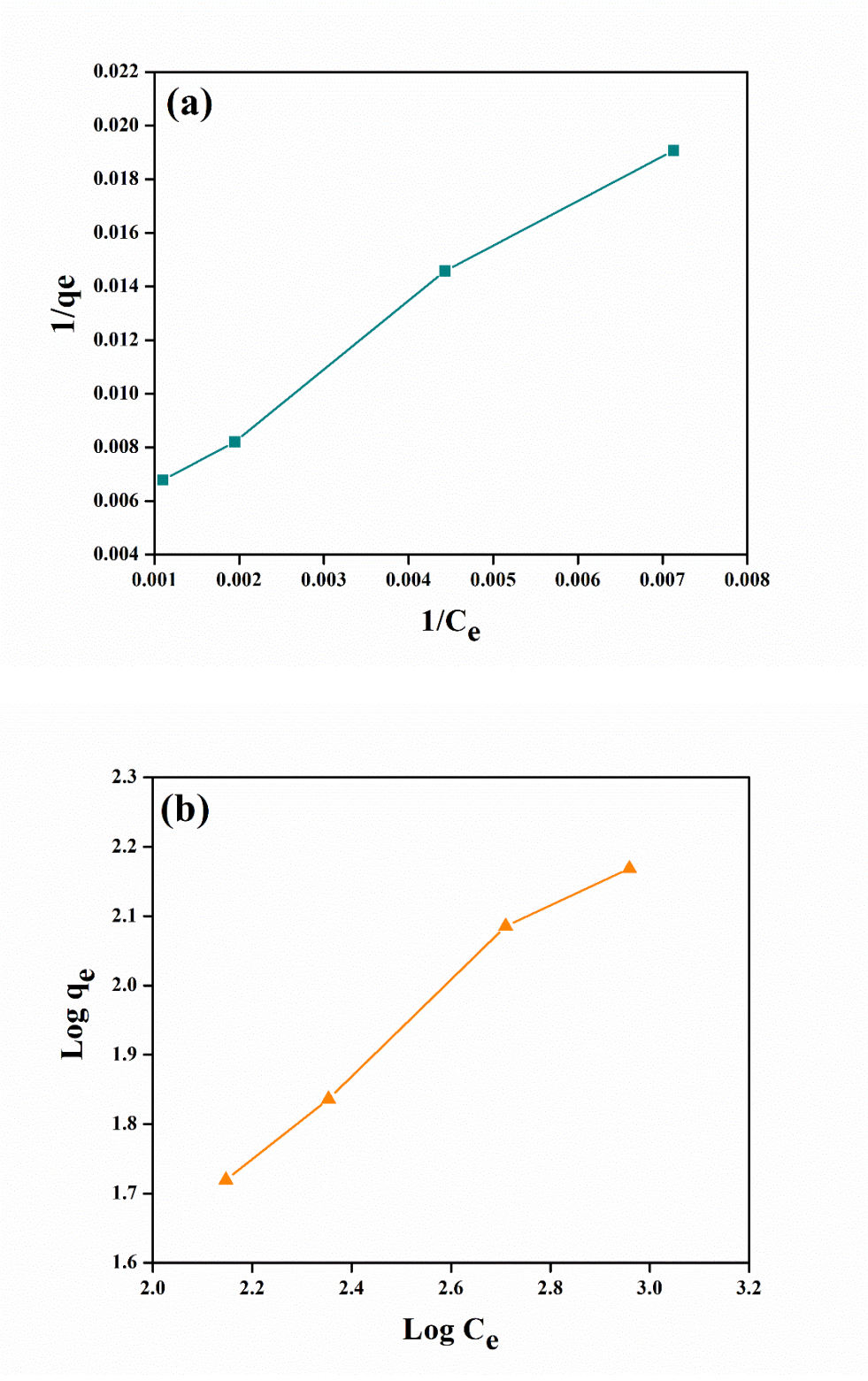

Fig. 7. (a) Langmuir models for adsorption of furfural by AC/nZVI nanoparticles; (b) Freundlich models for adsorption of furfural by AC/nZVI nanocomposites.

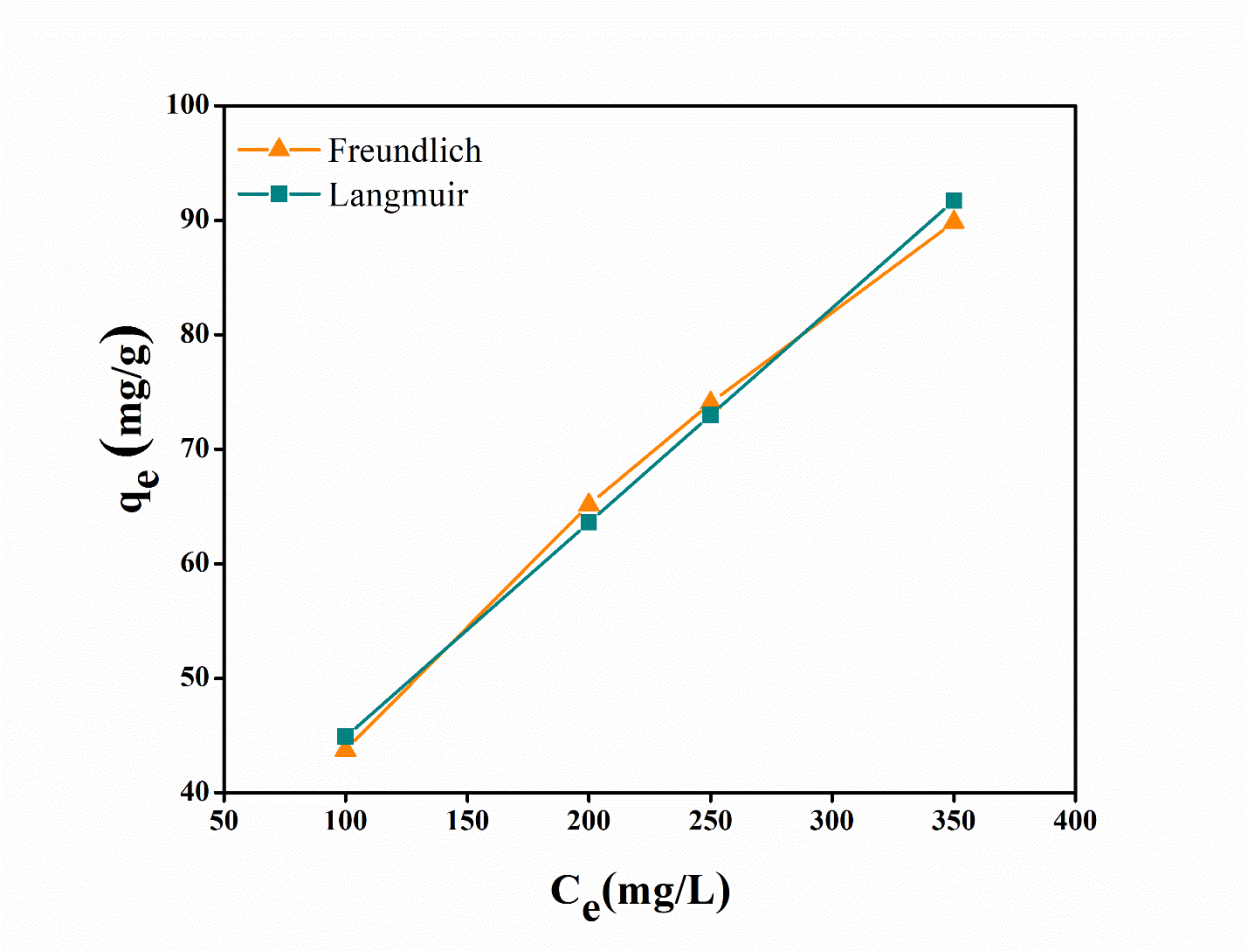

Fig. 8. Isotherm plots for furfural adsorption by AC/nZVI-NPs (pH = 7, dose = 4 g/L, C_0= 250 mg/L, Time=60 min, stirring speed = 250 rpm, and Temp = 25 ± 2˚C).

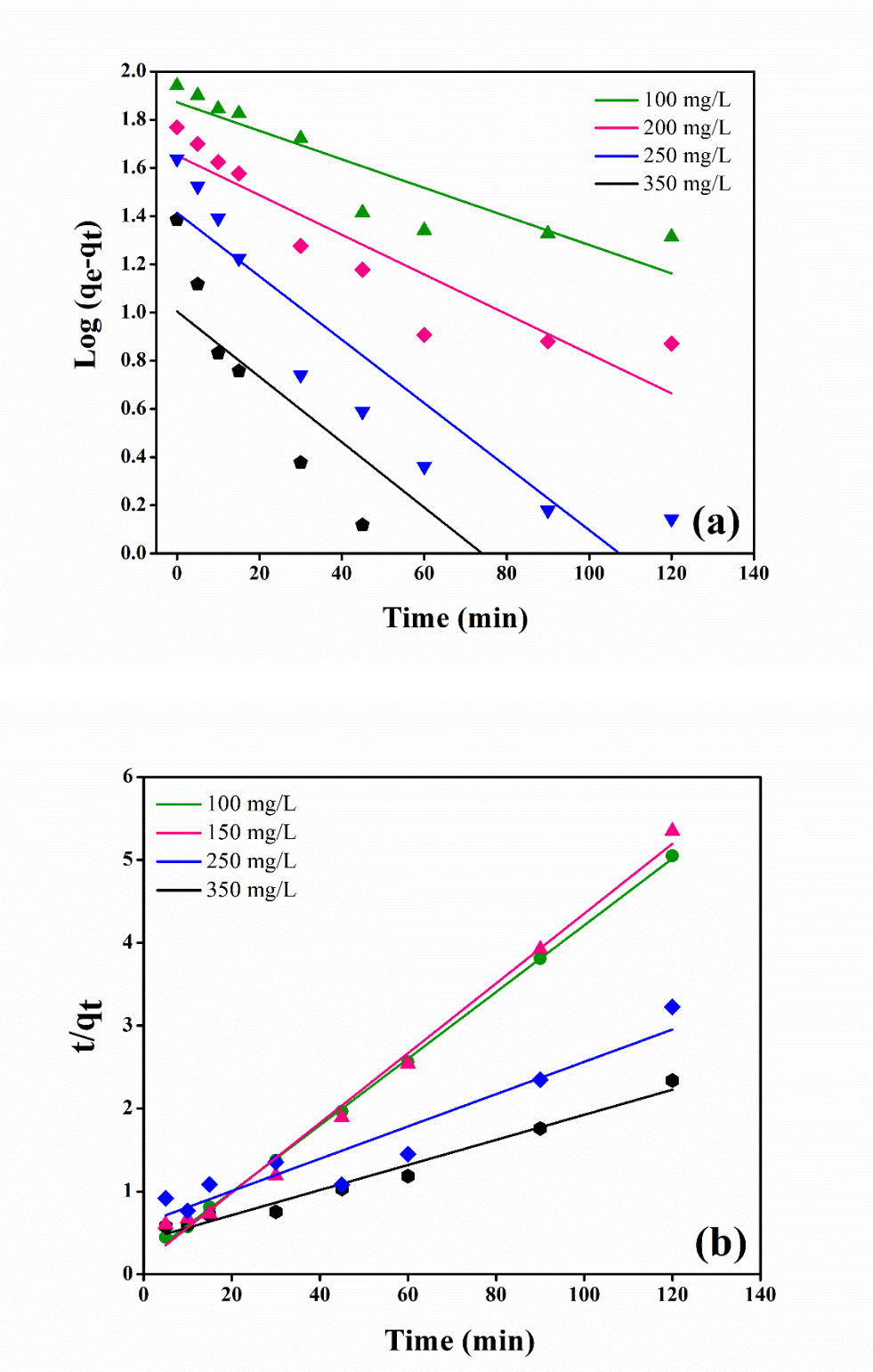

Fig. 9. (a) Pseudo first order kinetics models for the adsorption of furfural by AC/nZVI nanoparticles; (b) Kinetic mechanisms for Pseudo second order adsorption of furfural by AC/nZVI nanocomposites.

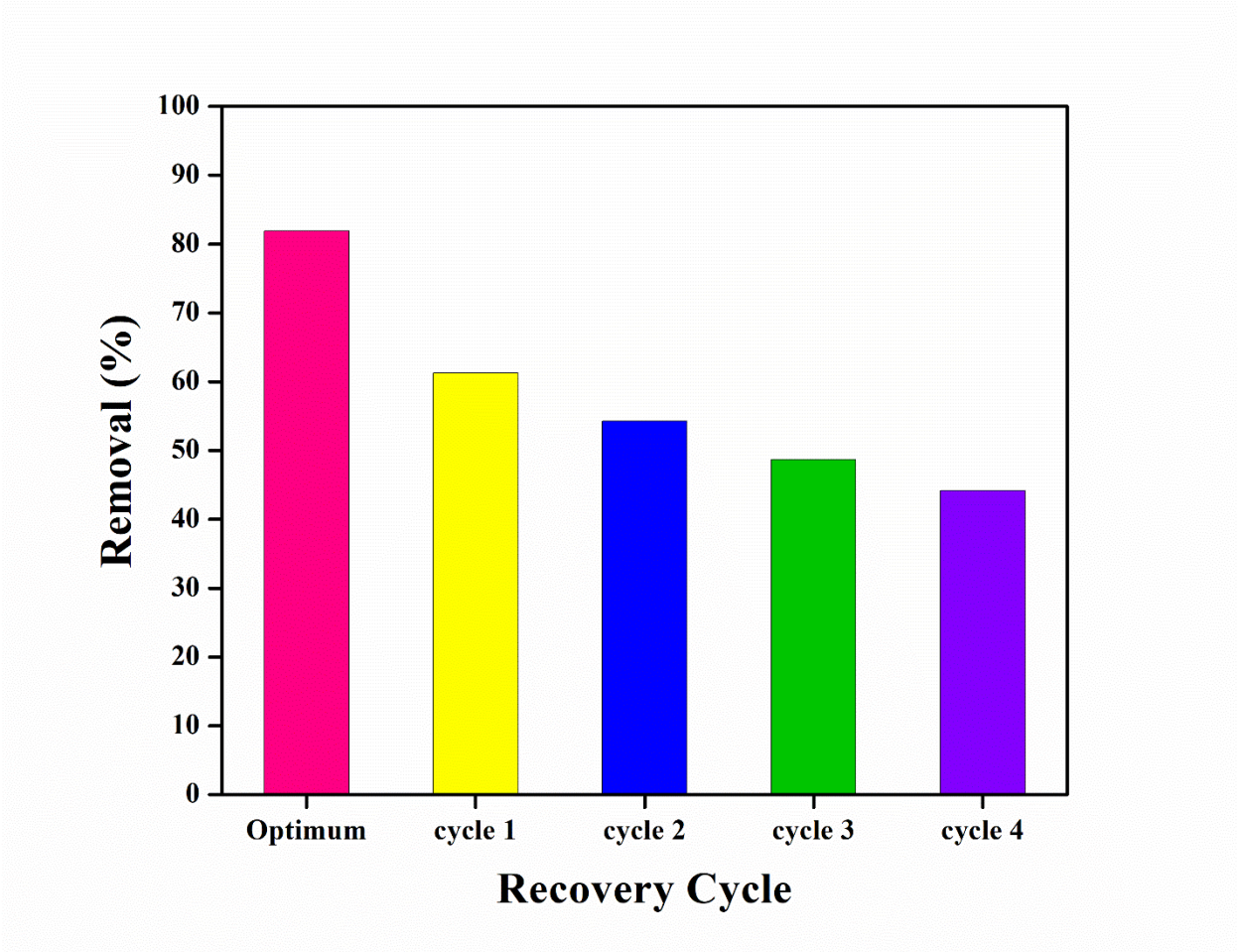

Fig. 10. The AC/nZVI nanoparticles recovery in four stages.

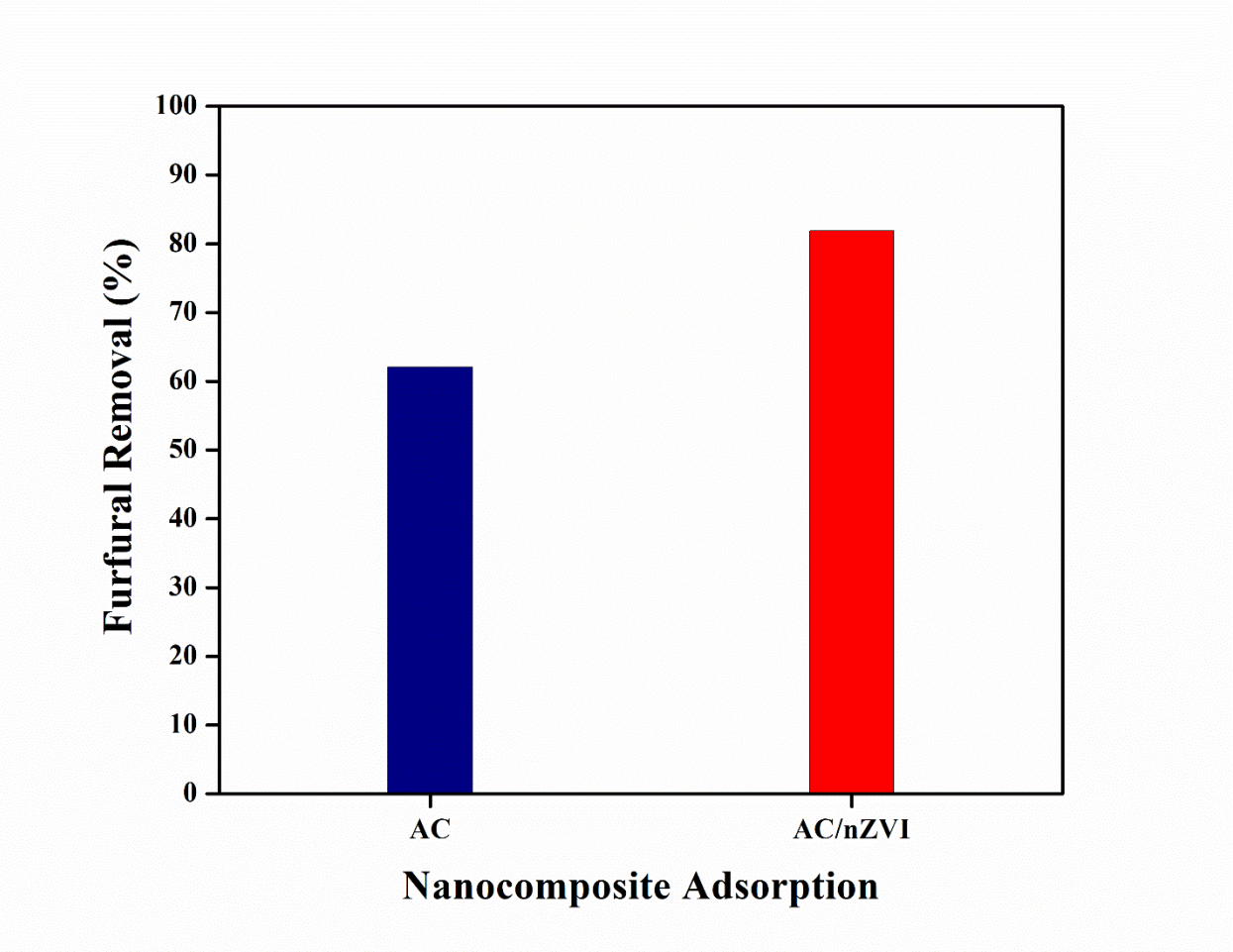

Fig. 11. Comparison of different processes on the adsorption of furfural (pH = 7, dose = 4 g/L, C_0 = 250 mg/L, Time = 60 min, stirring speed = 250 rpm, and Temperature = 25 ± 2^0C).